JOURNAL OF
EMERGING INVESTIGATORS

Article

Enhancing the quantum efficiency of a silicon solar cell using one dimensional thin film interferometry

Harsh Ahuja[1], Vinod Chacko[2]

[1] Heritage International Xperiential School, Gurgaon, Haryana, India

[2] Mahindra International School, Pune, Maharashtra, India

SUMMARY

Crystalline silicon solar cells are prominent renewable energy sources that convert solar energy into electrical energy without emitting greenhouse gases. They are used to energize satellites as well as provide electricity for buildings, local areas/settlements, and remote locations. However, the efficiency of these solar cells is limited by two factors: light reflection at the Si-Air interface, which reduces energy absorption, and the recombination rate of electron-hole pairs that reduces the mobile charge carriers available for electricity conduction. Solar cell expenses are comparable to conventional energy resources, motivating research to increase solar cell efficiency for commercial viability. The goal of our study was to increase crystalline solar cell efficiency theoretically by simulation. We mathematically simulated an omni-directional reflector with alternate Si/SiO_2 layers using multi-layered thin film interferometry in MATLAB, which was designed to reflect wavelengths in the range of 628 nm to 808 nm. We found that the ODR's energy reflected more energy at a central wavelength of 800 nm and 8 total layers. We also simulated an anti-reflection coating layer for the top of the solar cell using alternate ZnO-SiO_2 multilayers for enhanced transmission in the range of 481 nm to 2000 nm to increase solar cell efficiency for various optoelectronic devices and thermo-photovoltaic applications. We found that this reduced the reflectivity of the Si-Air interface by 49%.

INTRODUCTION

Solar cells are renewable and clean energy sources, being the third largest renewable global energy contributor behind hydropower and wind energy (1). Solar cells can be divided into three categories: crystalline silicon-based, thin film, and third generation solar cells (which are made of materials like gallium arsenide, amorphous silicon, and perovskite). Crystalline silicon is used widely for its durability, availability, and relatively lower cost (2). Crystalline silicon-based solar cells are further classified as monocrystalline (single silicon crystal) or polycrystalline (multiple silicon crystals) (3). The total global solar cell market is expanding and is expected to reach $508.18 billion by 2032 (4). A larger solar cell market implies greater adoption, and hence a reducing dependence on fossil fuels. However, crystalline solar cells specifically exhibit a low efficiency of 24-26%, which limits the environmental benefits of mass adoption of solar cells (5). To maximize these benefits, we must maximize the efficiency of the most widely used solar cell - crystalline solar cell.

Solar cells generate electricity through the liberation of electrons from the Silicon lattice by incident radiation. Electrons are always liberated from a specific part of the solar cell called the Depletion Layer (6). When these electrons are liberated, they leave behind gaps called holes. Both the electron and hole are meant to leave the solar cell through a wire (hence generating electricity), and join together outside the cell (a process called recombination). Together, an electron and hole are collectively termed an electron-hole pair (7). A solar cell's energy bandgap is the range of energy of photons necessary for liberating electrons from their parent atoms (8). Silicon solar cell bandgap is from 1.11 eV to 3.5 eV (1 eV=1.6 x 10^{-19} J) (9). All photons carry energy based on their wavelength, expressed as (10)

$$E_{photon} = \frac{hc}{\lambda} \quad (1)$$

where c is the speed of light in a vacuum (3 x 10^8 ms^{-1}) and h is Planck's constant (6.62 x 10^{-34} Js). Therefore, the crystalline silicon solar cell bandgap in terms of the wavelengths of incident photons that can generate electron-hole pairs, ranges from $\Delta\lambda_s$= 413 nm to 1117 nm (Eq. 1). When light falls on the depletion layer, photons with energy within this bandgap (range of wavelengths) are absorbed, and electron-hole pairs are generated.

Light is an electromagnetic wave which vibrates in directions perpendicular to the direction of the wave propagation. It is composed of oscillating electric and magnetic fields which are perpendicular to each other. The TE (Transverse Electric) mode is defined as an electromagnetic wave to which the oscillating electric field is always perpendicular to the direction of propagation. The TM (Transverse Magnetic) mode is defined as an electromagnetic wave to which the oscillating magnetic field is always perpendicular to the direction of propagation (11).

Crystalline silicon solar cells have limited efficiency because only 24-26% of incident solar energy can be used to generate electricity, while the remaining energy is either reflected at the Si-Air interface, or transmitted without creating any new electron-hole pairs, and therefore not generating electricity (12). Solar cell efficiency is further reduced due to recombination of some electron hole pairs, a process that releases the same energy that initially caused the electrons and holes to separate, in the form of a photon (13). Thus, increasing light absorption is important to improve solar cell efficiency. One method of increasing light absorption is by photon recycling (14). Photon recycling involves redirecting photons that are emitted during recombination or transmitted from the solar cell back into its depletion layer by reflection. Photons that successfully reach the depletion layer liberate

https://doi.org/10.59720/23-023

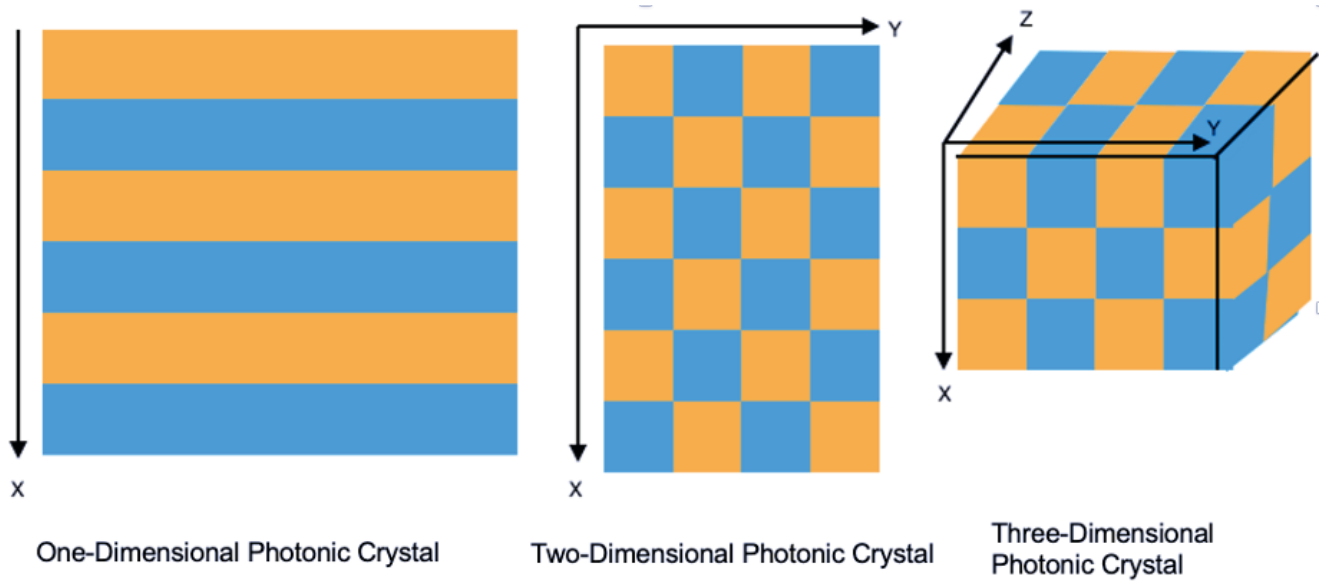

Figure 1: One, two and three dimensional photonic crystals. Differently colored regions are regions with different refractive indices. The apparent equality of thickness between layers is not to scale. The rightmost figure showcases a 1DPC, where refractive index and layer thickness change with respect to only one axis, and is constant with respect to the other two. The central and leftmost figures extend the variation in refractive index and thickness to 2 axes (2DPC) and 3 axes (3DPC), respectively.

electron hole pairs once again and make them available for conduction. This process increases the efficiency of the solar cell. At the same time, increasing the transmission of light by reducing reflection at the Si-Air interface is also important to improve solar cell efficiency. We can design effective reflectors and transmitters to facilitate this through the application of photonic crystals (PCs) through simulation.

PCs are multi-layered dielectric structures in which there is a periodic variation of refractive index between a high and low value **(Figure 1)**. A one-dimensional PC (1DPC) displays these variations in refractive index along one axis. It is also easier to manufacture and can be mathematically modelled with few approximations and assumptions (15). Due to the variations in refractive index, the 1DPC prohibits certain ranges of photon wavelengths, called bandgaps, from propagating through it (16). The photons with wavelengths in the 1DPC's bandgap are reflected by it.

When light is incident from air on a dielectric thin film of refractive index of a certain thickness and refractive index, it is partly reflected from the top and bottom surface of the thin film (17). The two reflected waves interfere to give the resultant intensity of reflected light from the thin film. There is also a phase change of π between the two reflected waves, as one of them is reflected while going from rarer medium to denser medium. There may be two phase changes if the second layer of the 1DPC is denser than the first. When the two waves interfere destructively, the film operates as an ARC by preventing transmission of outgoing waves. When they interfere constructively, the film operates as a reflector since the amplitude of outgoing waves is amplified.

Through suitable selection of design parameters of a 1DPC, we can modulate this bandgap region for both angle of incidence and polarisation to act as both a reflector and a transmitter in the effective solar wavelength region (18).

To increase the efficiency of a solar cell, we theoretically designed and simulated an omni-directional reflector (ODR) using a 1DPC of alternating Si and SiO_2 layers, positioned on the back side of a solar cell to reflect wavelengths within $\Delta\lambda_s$ (Eq. 1) for all angles of incidence and states of polarization (19, 20-23). This can provide transmitted photons and photons emitted by recombination another chance to be absorbed by reflecting them back into the depletion layer. We also theoretically designed and simulated an anti-reflectional coating (ARC) using a 1DPC of alternating ZnO and SiO_2 layers to enhance the transmission properties of light at the Si-Air interface of crystalline silicon solar cells. ZnO was chosen as a material for the ARC for its high transparency in the visible wavelength range (24). We hypothesized that we could increase the solar cell qualitative efficiency by enhancing reflection of otherwise transmitted photons at the rear end of a crystalline solar cell through the application of an ODR and increasing light transmission at the front Si-Air interface through the application of an ARC. We found that a solar cell retrofitted with an ARC of eight layers, designed at a central wavelength of 400 nm and an ODR with eight layers, designed at an 800 nm central wavelength, would qualitative yield higher efficiency.

RESULTS

In our proposed structure, we configured an ARC at the front light-facing surface of the solar cell and also introduced and ODR at the rear end of the solar cell **(Figure 2)**. We measured the reflection spectrum for the ODR **(Figure 3)**. We found that a lower central wavelength for the ODR is more efficient than a higher one since the resultant bandgap reflects more energy. We compared the energy reflected from an ODR designed for a central wavelength of 800 nm to one for 1200 nm. At central wavelength 800 nm, the ODR bandgap is 628 nm - 808 nm **(Figure 3) (Appendix 2)**, reflecting 5.01×10^{-12} J. In comparison, at central wavelength 1200 nm with band edges 945 nm - 1206 nm **(Figure 4) (Appendix 2)**, 4.85×10^{-12} J is reflected. We observed a significant 3.5%

https://doi.org/10.59720/23-023

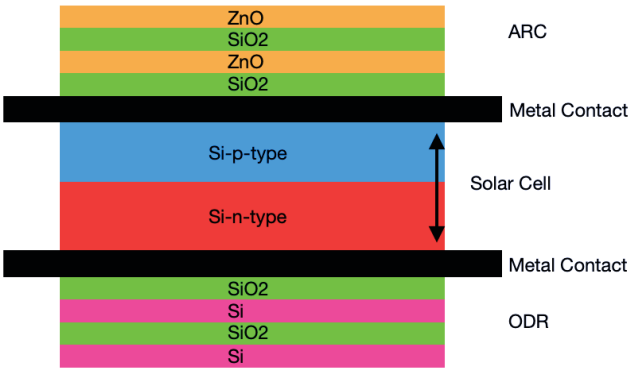

Figure 2: A Solar Cell fitted with contacts, an ODR and an ARC. Sunlight is ideally first incident on the ARC, which is the alternating stack of orange (ZnO) and green (SiO2) layers. The alternating stack of pink (Si) and green layers (SiO_2) is the ODR. Black layers are metal contacts fit to the upper and lower surfaces of the p-n junction (red and blue layers between the metal contacts). The current graphic representation is meant to situate the ODR and ARC with respect to the solar cell, and not to perfectly represent the interior structure of a Monocrystalline Silicon solar cell.

increase in the energy reflected from the ODR for the same design parameters, at a central wavelength of 800 nm instead of 1200 nm. When scaled up to multiple solar cells, this quantity is more significant. The ODR bandgap sharpens with more layers, increasing efficacy but also causing absorption losses and fabrication challenges. The 100% reflection band width increases as the number of layers N increases from 2 to 10 for TE and TM modes **(Figure 5)**.

Based on our simulation, we observed a high transmission region for the ARC from 481 nm to 2000 nm **(Figure 6)**. To assess the ARC's effectiveness, we compared the reflection spectrum for the Si-Air interface without the ARC, with that of the ARC **(Figure 7)**. We observed that the Si-Air interface gives a large reflection in wavelength range 248 nm – 1000 nm, with an average reflectance of 64% within the silicon solar cell bandgap ($\Delta\lambda_s$), whereas the ARC has an average reflectance of 15% in the same region. This means that only 36% percent of incident solar energy is transmitted at the Si-Air interface without the ARC. A solar cell with the ARC will transmit 85% percent of incident radiation, which is 49% more than the Si-Air interface without the ARC.

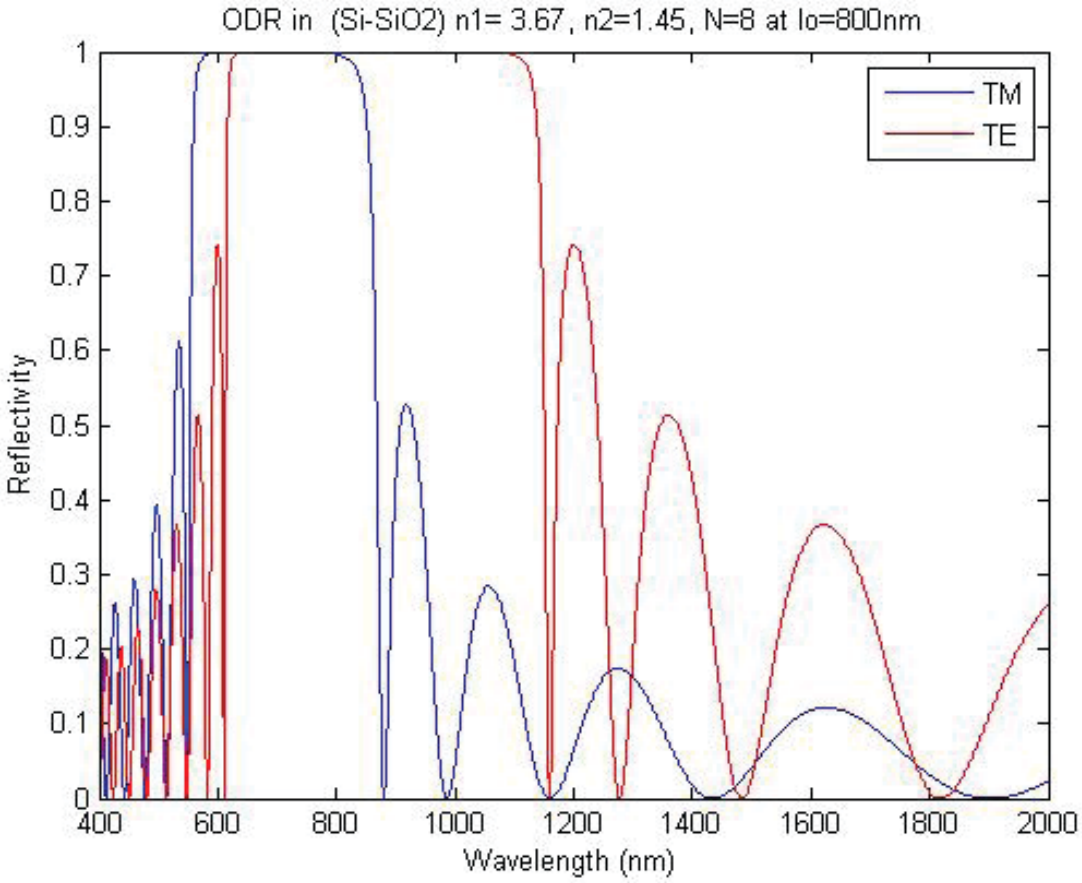

Figure 3: ODR in ($Si-SiO_2$) n1=3.67, n2=1.45, N=8, at lo=800 nm. Reflection spectrum for Si/SiO_2 for eight layers in (blue) TM mode, θ=90° (red) TE mode, θ=0°, for wavelength range of 400 – 2000 nm. TE is Transverse Electric. TM is Transverse Magnetic. The reflection spectrum was generated on MATLAB with input parameters as eight layers and central wavelength 800 nm. The ODR bandgap with 100% reflectance is 628 – 808 nm.

https://doi.org/10.59720/23-023

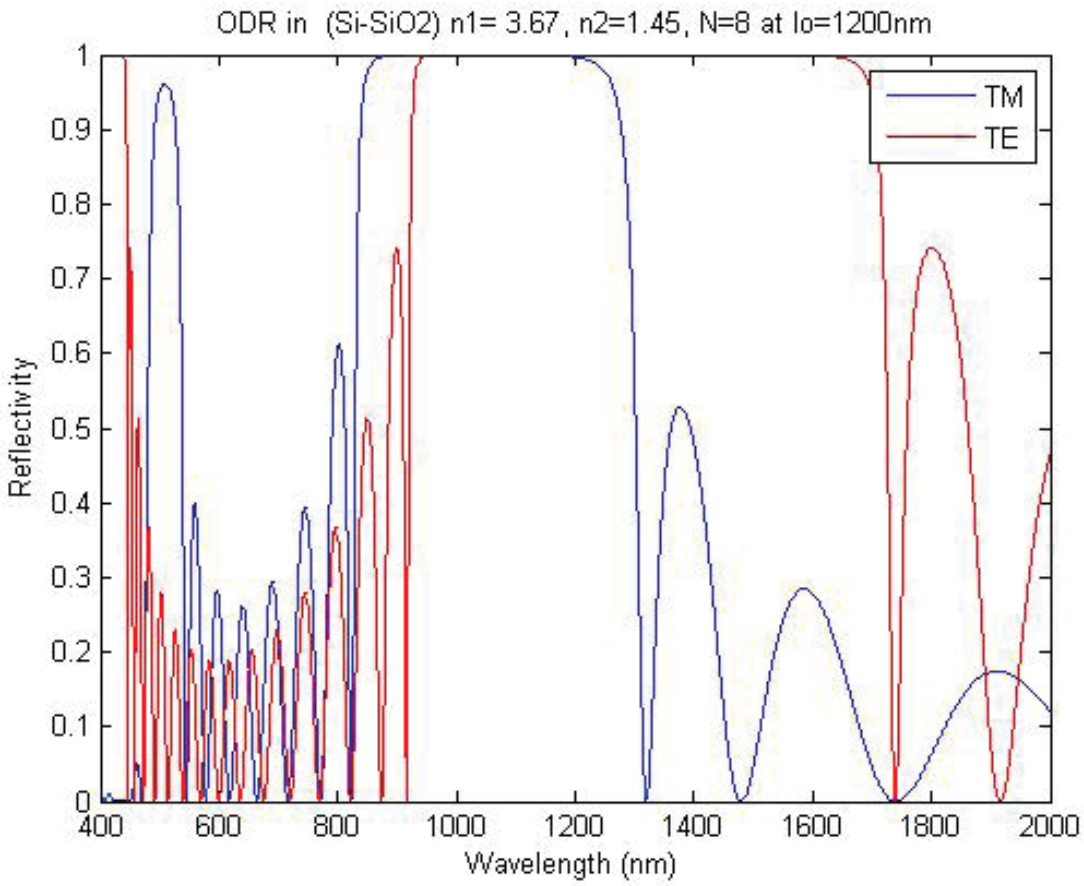

Figure 4: ODR in (Si-SiO_2) n1=3.67, n2=1.45, N=8, at lo=1200 nm. This is the ODR Reflectance spectrum at central wavelength of 1200 nm, for TE mode (θ=0°) and TM mode (θ=90°) in Si/SiO_2. TE is Transverse Electric. TM is Transverse Magnetic. A MATLAB simulation with input parameters of eight layers and central wavelength as 1200 nm was used to generate spectrum. The ODR bandgap of 100% reflectance was from 945 to 1206 nm.

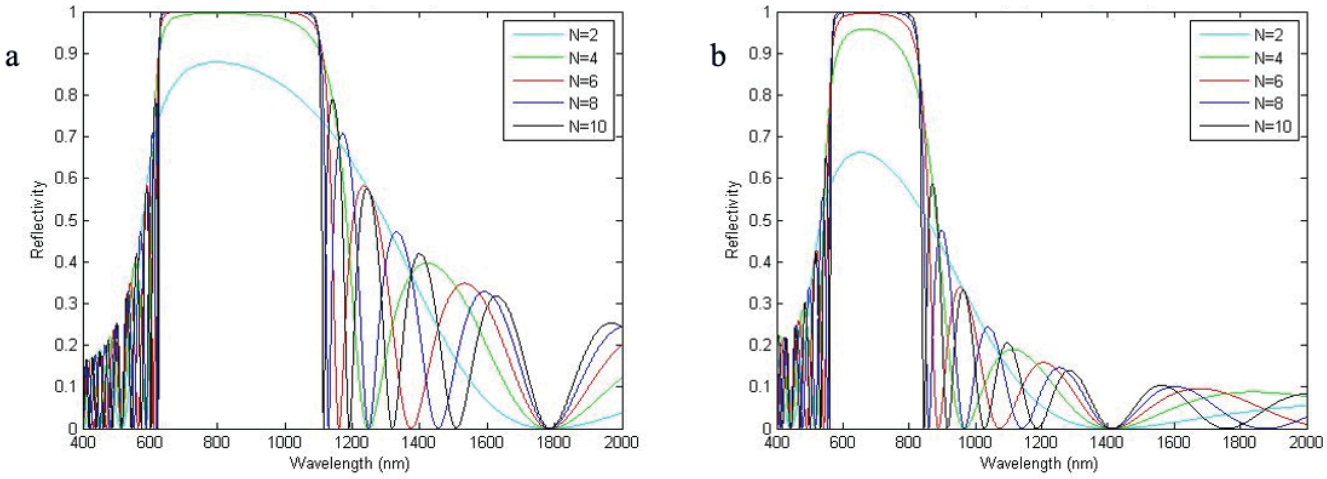

Figure 5: (a) Effect of number of layers on Reflectivity spectrum (Si-SiO_2) TE normal incidence : N=2,4,6,8,10. (b) Effect of number of layers on Reflectivity spectrum (Si-SiO_2) TM theta=90 : N=2,4,6,8,10. TE is Transverse Electric. TM is Transverse Magnetic. Reflection spectrum for Si-SiO_2, θ=0° for N=2, 4, 6, 8 and 10. A MATLAB simulation with input parameters of 2, 4, 6, 8 and 10 layers was used to graph reflection spectra for all inputs collectively on graph.

https://doi.org/10.59720/23-023

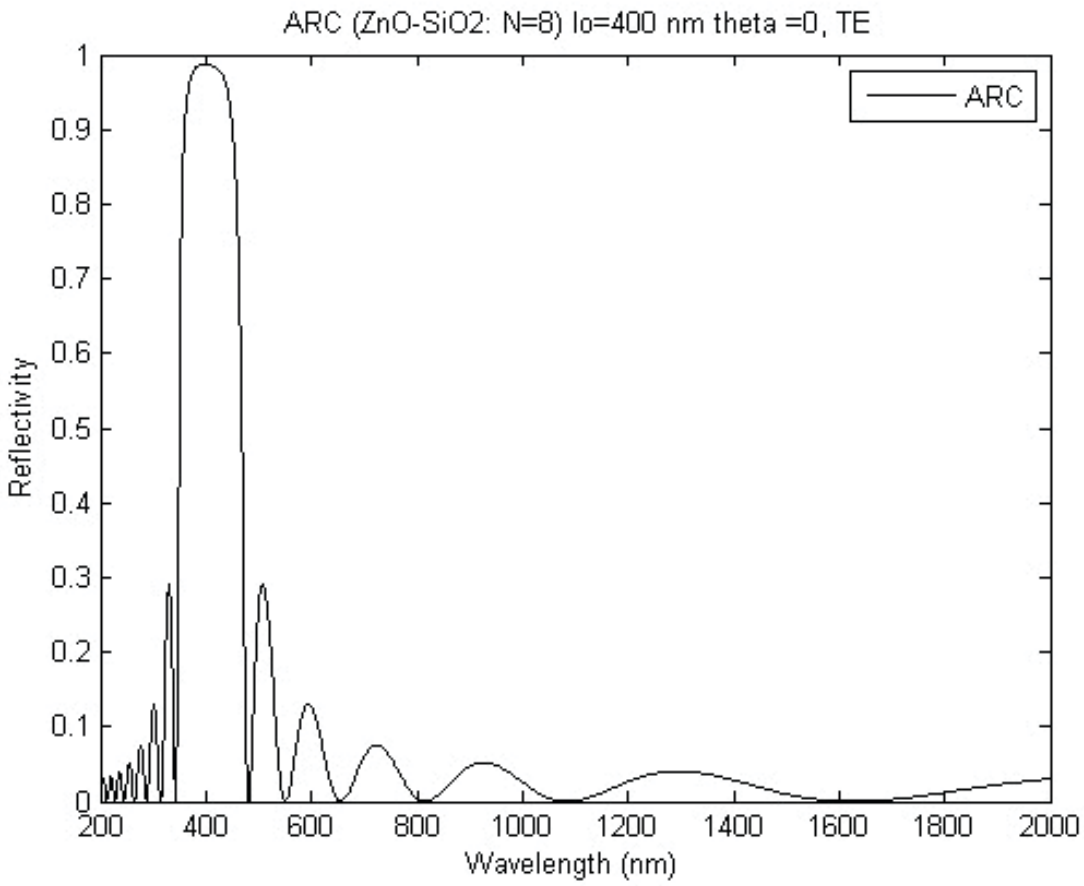

Figure 6: ARC (ZnO-SiO2: N=8) lo=400nm theta=0, TE. The reflection spectrum for ZnO/SiO2 ARC at θ=0°. TE is Transverse Electric A MATLAB simulation with input parameters as eight layers and central wavelength 400 nm was used to generate the spectrum. The ARC bandgap with 100% reflectance is from 342 nm – 481 nm for 400 nm central wavelength.

DISCUSSION

We hypothesized that the attachment of an ODR to a solar cell could successfully increase the recycling of photons that are typically lost due to recombination or transmittance in it for reabsorption, and that the attachment of an ARC to a solar cell could increase its surface transmittance of a Si-Air Interface. The ODR demonstrated a high reflectance bandgap of 628 nm – 808 nm, and the ARC demonstrated a high-transmission range of 481 nm – 2000 nm. Increasing the central wavelength for the ARC broadened its high reflection bandgap (23), causing more energy losses. The ARC transmittance range at central wavelength of 400 nm spans the silicon solar cell bandgap ($\Delta\lambda_s$), and so it is a highly appropriate central wavelength to maintain. Finally, the ARC bandgap does not overlap with the ODR's bandgap, meaning the light that the ODR is meant to recycle is not reflected prematurely by the ARC and reaches the ODR. A significant portion of this radiation was previously reflected by the Si-Air interface but is now transmitted and recycled by the solar cell. The ARC exhibits a high transmission region that increases surface transmittance for the entire silicon solar cell bandgap, as hypothesized.

The ODR is placed suitably at the rear end of the solar cell, after the metal contact **(Figure 2)**. It reflects the photons that the solar cell does not absorb, or which are emitted by recombination, back into the depletion layer to generate more charge carriers and increase efficiency. Constantly increasing solar cell thickness does not lead to 100% absorption (25). While more light is indeed absorbed, the amount of recombination increases concurrently, since recombination is only possible after absorption. The parallel increase in radiation losses means that 100% absorption is an impractical extreme and unlikely to be attained (26).

The study was empirically constrained due to the manufacturing difficulty of 1DPCs. This is because 1DPCs are manufactured at the nanoscale level, and the precise layer thickness requirements are difficult to control, due to which experimental uncertainty is high. Future research should Investigate effects of temperature on the bandgap, as temperature changes both material thickness and refractive index and hence bandgap width (27, 28). These changes warrant exploration in the context of a solar cell's operation at multiple temperatures, with the temperature-response of an attached ODR and ARC. In conclusion, we observed in this study that an ARC designed from ZnO/SiO_2 multilayers with a central wavelength of 400 nm and eight layers, and an ODR designed from Si/SiO_2 with a central wavelength of 800 nm and eight layers, are capable of qualitatively increasing the efficiency of a conventional Silicon solar cell. In the context of burgeoning solar cell adoption, it is imperative that efficiency is

https://doi.org/10.59720/23-023

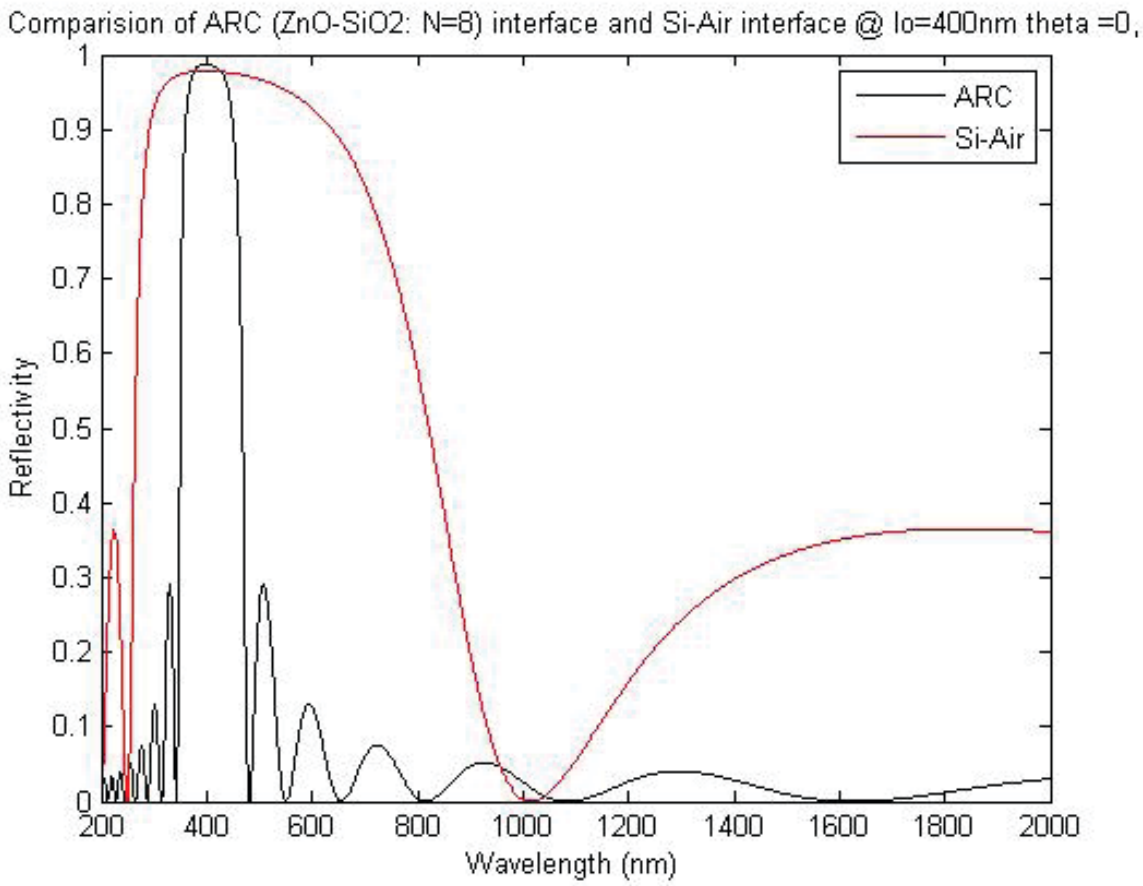

Figure 7: Comparison of ARC (ZnO-SiO_2: N=8) and Si-Air interface at lo=400 nm theta=0. Si-Air interface and ARC reflection spectrum for normal incidence at θ=0°. A MATLAB simulation with input parameters as eight layers, refractive index 1 as 2.08, refractive index 2 as 1.45 and central wavelength 400 nm used for ARC, and 2 layers, refractive index 1 as 1.00, refractive index 2 as 3.67 and central wavelength 400 nm for Si-Air interface, was used to generate both reflection spectra.

increased as much as it can at an early stage, since attempts to enhance efficiency for a large-scale grid of solar power would carry high costs in a short period of time. Given that the solar cell market is currently much smaller than the fossil fuel market, research in efficiency-increasing mechanisms such as ARCs and ODRs is well-timed and important.

MATERIALS AND METHODS

The Quarter Wave-Stack Condition

For normal incidence, the optical path difference between the two waves reflected by a thin film of thickness *d* and refractive index *n* is *2dn*. The two reflected waves interfere according to the following conditions for constructive (superposition of waves that are in phase, yielding high intensity of light.) and destructive interference (superposition of waves that are out of phase, yielding light of low intensity.) (Eq. 2) (Eq. 3) (17)

$$2dn = \left(m + \frac{1}{2}\right)\lambda \quad (2)$$

$$2dn = m\lambda \quad (3)$$

Where m is an integer ≥ 0, the reflected intensity through the thin film will show constructive interference for minimum thickness of the thin film (m = 0) and thus (Eq. 4) becomes the quarter-wave stack condition in reflection mode, where λ_0 is the wavelength of light in air.

$$4dn = \lambda_0 \quad (4)$$

To design the ODR and ARC through simulation, we followed a previously published protocol (14) (23) (29) (30). While this protocol is applied in general for designing an ODR using the transfer matrix method (14), this paper focuses on the application of such an ODR on the backside of a solar cell to improve its efficiency. In this paper, we design the ODR and ARC through this method to improve the efficiency of the solar cell.

Generation of the Reflection Spectrum of the ODR and ARC

A MATLAB Simulation was used to generate the bandgap of the ODR and ARC (31) **(Appendix 1)**. The Software accepted the parameters of the two refractive indices of a 1DPC's two layers, the total number of layers, the central wavelength and whether the computation was to be conducted for TE or TM modes at 0° for TE and 90° for TM. Both bandgaps were generated concurrently on the same graph by the software.

https://doi.org/10.59720/23-023

For the ODR, we used the refractive indices of 3.67 and 1.45, eight layers as the total number of layers and 800 nm as the central wavelength, as inputs for this software. We used the quarter wave stack condition to design the ODR and to calculate layer thickness. We also used the classical wave equation with periodic boundary conditions to determine the reflection coefficient of a multilayered 1DPC using the transfer matrix method or both transverse electric (TE) and transverse magnetic (TM) modes (Eq. 20) (23). The wavelength layer for 100% reflection is an overlap of the reflection spectra of TE at θ=0° and TM at θ=90° and is called the ODR bandgap (14). For this study, we chose to maintain a central wavelength of 800 nm. We chose to simulate an eight--layered one-dimensional structure of Si and SiO_2. We set the total number of layers to reduce the fabrication challenges of a greater number of layers (32) and because the ODR bandgap width decreases only marginally after eight layers **(Figure 5)**. The refractive indices of Si and SiO_2 are 3.67 and 1.45 at 800 nm, respectively (33, 34). We computed layer thickness from the quarter wave-stack condition(Eq. 4): The thicknesses of the Si and SiO_2 layer were 58.495 nm and 137.93 nm, respectively.

For the ARC, we used the refractive indices of 2.08 (ZnO) and 1.45 (SiO_2) as inputs, eight layers as the total number of layers and 400 nm as the central wavelength, as inputs for this software. We used another multi-layered structure of 8 alternate layers of ZnO (with thickness 48.07 nm) and SiO_2 (with thickness 68.96 nm) for the ARC (34). We set The central wavelength, which is the wavelength at which reflectance is 100%, at 400 nm to maintain a narrow bandgap. We calculated the thickness of layers in ARC using the quarter wave stack condition. We computed the reflection data for this ARC structure at normal incidence for TE and TM modes **(Table 2)**.

We also employed this MATLAB simulation to determine the reflectivity characteristics of the Si-Air interface, for which we used the refractive indices of 1 and 3.67, with a total of two layers, and central wavelength of 400 nm.

The bandgap for the ODR, ARC and Si-Air interface was determined from the lower edge of the TE mode bandedge and the upper edge of the TM mode bandgap.

The MATLAB simulation used is based on the following mathematical framework, wherein a periodic dielectric medium is characterised with alternating high and low refractive index mediums (14).

$$n(x) = \begin{cases} n_2, & 0 < x < a \\ n_1, & -b < x < 0 \end{cases} \quad (8)$$

The classical wave equation for the electric field in electromagnetic solar radiation, for both high and low refractive index layers is considered

$$\frac{d^2E}{dx^2} + \frac{n_i^2\omega^2}{c^2}E = 0 \quad (i = 1, 2, ..) \quad (9)$$

Where ω is the angular frequency and c is the speed of light. The following boundary conditions of continuity (Eq. 10-13) at the interface of the two different mediums are also used to determine the solutions of the wave equations (Eq. 14-16).

$$E_1(-b) = E_2(-b) \quad (10)$$

$$\frac{dE_1(-b)}{dx} = \frac{dE_2(-b)}{dx} \quad (11)$$

$$E_1(0) = E_3(0) \quad (12)$$

$$\frac{dE_1(0)}{dx} = \frac{dE_3(0)}{dx} \quad (13)$$

The obtained solutions to the wave equation are of the form

$$E_1(x) = A_1 e^{i\alpha x} + B_1 e^{-i\alpha x} \quad (-b < x < 0) \quad (14)$$

$$E_2(x) = A_2 e^{i\beta x} + B_2 e^{-i\beta x} \quad (-(b+a) < x < -b) \quad (15)$$

$$E_3(x) = A_3 e^{i\alpha x} + B_3 e^{-i\alpha x} \quad (0 < x < a) \quad (16)$$

Where A_1, A_2, A_3 and B_1, B_2, B_3 are the electric field

(ODR)Si/SiO_2	TE			TM		
	Lower Bandgap Edge/nm	Upper Bandgap Edge/nm	Bandgap/nm	Lower Bandgap Edge/nm	Upper Bandgap Edge/nm	Bandgap/nm
$\theta = 0^o$	628	1090	462	628	1090	462
$\theta = 90^o$	501	1036	535	585	808	223

Table 1: These are the upper and lower edges of the bandgap for TE and TM modes in an eight-layered Si/SiO_2 photonic crystal, generated on a MATLAB Simulation with input parameters as eight layers and central wavelength 800 nm to generate the reflectance spectrum. These values were determined directly from the software-generated figure. TE is Transverse Electric. TM is Transverse Magnetic. The ODR bandgap with 100% reflectance, between TE (θ=0°) and TM(θ=90°), is from 628 nm – 808 nm.

(ARC)ZnO/SiO_2	TE			TM		
	Lower Bandgap Edge/nm	Upper Bandgap Edge/nm	Bandgap/nm	Lower Bandgap Edge/nm	Upper Bandgap Edge/nm	Bandgap/nm
$\theta = 0^o$	342	481	139	342	481	139

Table 2: These are the TE and TM mode band edges for ZnO/SiO_2 at θ=0°. TE is Transverse Electric. TM is Transverse Magnetic. A MATLAB simulation with input parameters of eight layers and central wavelength as 400 nm was used to generate spectrum. The ARC bandgap with 100% reflectance is from 342 nm – 481 nm.

https://doi.org/10.59720/23-023

coefficients for transmitted and reflected waves in the corresponding region respectively, and $\beta=(n_2\omega)/c$ and $\alpha=(n_1\omega)/c$. The Bloch theorem (Eq. 17) is used for the boundary conditions of periodicity between the layers.

$$e^{iKd}E(x) = E(x+d) \quad (17)$$

The Bloch wavevector K is defined differently for TE and TM modes. The field coefficients of the first layer are linked to the field coefficients of the N^{th} layer through the Transfer Matrix Method (Eq. 18) using the continuous and periodic boundary conditions.

$$\begin{pmatrix} A_0 \\ B_0 \end{pmatrix} = T_1 T_2 \dots T_N \begin{pmatrix} A_N \\ B_N \end{pmatrix} \quad (18)$$

The reflection coefficient is calculated as the ratio of the field coefficients of the reflected and incident ray at the first layer considering the transmission coefficient of the N^{th} layer, A_N=0 and the reflection coefficient of the Nth layer, B_N=1.

$$r_N = \frac{B_0}{A_0} \quad (19)$$

$$R_N = |r_N|^2 \quad (20)$$

We designed the MATLAB simulation to carry out this mathematical framework, in order to calculate the value of the reflection coefficient, for each wavelength in a desired wavelength range, using the known design parameters of refractive index, layer thickness, angle of incidence and mode of vibration (Eq. 20) **(Appendix 1)**.

Calculation of the Energy Reflected by the Bandgap of the ODR at Different Central Wavelengths

We calculated the energy reflected from the bandgap, $\varepsilon(\lambda_L,\lambda_U)$, with the help of the following equations

$$\varepsilon(\lambda_L,\lambda_U) = \sum_{i=\lambda_L}^{\lambda_U} \frac{hc}{i} \quad (5)$$

$$\varepsilon_{800\,nm} = 5.01 \times 10^{-12}\ \text{J} \quad (6)$$

$$\varepsilon_{1200\,nm} = 4.85 \times 10^{-12}\ \text{J} \quad (7)$$

where λ_L, λ_U are the upper and lower band-edges, h is Planck's constant and c is the speed of light.

We converted these equations into a MATLAB program (Appendix 2). Then, we used the ODR's bandgap's edges as inputs for the lower and upper wavelength λ_L and λ_U. The program then yielded the value of the total energy reflected by the ODR's bandgap. We did this for both the reflection spectra of the ODR at 800nm and 1200nm central wavelength **(Figure 3) (Figure 4)**.

Received: January 30, 2023
Accepted: August 15, 2023
Published: May 3, 2024

REFERENCES

1. Bojek, P. "Solar PV." *International Energy Agency,* September 2022, www.iea.org/reports/solar-pv. Accessed 9 March 2024.
2. "What are Solar Cells?(Including Types, Efficiency and Developments)." *TWI,* www.twi-global.com/technical-knowledge/faqs/what-are-solar-cells. Accessed 9 March 2024.
3. "Solar Photovoltaic Cell Basics." *Office of Energy Efficiency & Renewable Energy,* www.energy.gov/eere/solar/solar-photovoltaic-cell-basics#:~:text=Silicon,of%20the%20modules%20sold%20today. Accessed 9 March 2024.
4. "Solar Cell Market." *Precedence Research,* October 2022. www.precedenceresearch.com/solar-cell-market. Accessed 9 March 2024.
5. "Best Research-Cell Efficiency Chart." *NREL,* www.nrel.gov/pv/cell-efficiency.html. Accessed 9 March 2024.
6. "Formation of a P-N Junction." *PVEducation,* www.pveducation.org/pvcdrom/pn-junctions/formation-of-a-pn-junction#:~:text=P%2Dn%20junctions%20are%20formed%20by,to%20the%20p%2Dtype%20side. Accessed 9 March 2024.
7. "Light Generated Current." *PVEducation,* www.pveducation.org/pvcdrom/solar-cell-operation/light-generated-current. Accessed 9 March 2024.
8. "Band Gap." *PVEducation,* www.pveducation.org/pvcdrom/pn-junctions/band-gap. Accessed 9 March 2024.
9. "Spectral Response." *PVEducation,* www.pveducation.org/pvcdrom/solar-cell-operation/spectral-response. Accessed 9 March 2024.
10. Tsokos, K.A. *Physics for the IB Diploma.* Cambridge University Press, 6th edition, 2014, pp. 271, Accessed 9 March 2024.
11. "Understanding TEM, TE and TM Waveguide Modes." *PRECISION Millimeter Wave,* precisionmmw.com/understanding-tem-te-and-tm-waveguide-modes/. Accessed 9 March 2024.
12. "Solar Cell Design Principles." *PVEducation,* www.pveducation.org/pvcdrom/design-of-silicon-cells/solar-cell-design-principles. Accessed 9 March 2024.
13. "Solar Performance and Efficiency." *Office of Energy Efficiency & Renewable Energy,* www.energy.gov/eere/solar/solar-performance-and-efficiency#:~:text=Direct%20recombination%2C%20in%20which%20light,fundamental%20factors%20that%20limits%20efficiency. Accessed 9 March 2024.
14. Raja, W., *et al.* "Photon recycling in perovskite solar cells and its impact on device design." *Nanophotonics,* vol. 10, no. 8, 27 May 2021, pp. 2023-2042. https://doi.org/10.1515/nanoph-2021-0067.
15. Chacko, V., *et al.* "Broad inhibition of Transmission Frequency in Multilayered Dielectric One Dimensional Photonic Crystal Nanostructure." *International Journal of Science and Engineering,* vol. 13, no. 1, 18 March 2019, pp. 7-11.
16. Banerjee, A. "Novel applications of one dimensional photonic crystal in optical buffering and optical time division multiplexing." *Optik,* vol. 122, no. 4, 16 September 2010, pp. 355-357. https://doi.org/10.1016/j.ijleo.2010.03.001.
17. Tsokos, K.A. *Physics for the IB Diploma. 6th edition,* Cambridge University Press, 2014, pp. 372-373, Accessed 9 March 2024.
18. Anishkumar, S. and Antony, A. "Tuneable and spectrally selective broadband reflector-Modulated photonic crystals and its application in solar cells." *Solar Energy,* vol. 162, 13 February 2018, pp. 525-532. https://doi.

https://doi.org/10.59720/23-023

org/10.1016/j.solener.2018.01.061.
19. Yablonovitch, S. E. "Inhibited Spontaneous Emission in Solid-State Physics and Electronics." *Physical Review Letters,* vol. 58, no. 20, 18 May 1987, https://doi.org/10.1103/PhysRevLett.58.2059.
20. John, S. "Strong localization of photons in certain disordered dielectric super lattices" Physical Review Letter, vol. 58, no. 23, 8 June 1987, https://doi.org/10.1103/PhysRevLett.58.2486.
21. Joannopoulos J. D., *et al.* "Photonic crystals: putting a new twist on light" *Nature,* vol. 386, 13 March 1997, pp. 143-149. https://doi.org/10.1038/386143a0.
22. Yuan K., *et al.* "Design of omnidirectional and multiple channeled filters using one-dimensional photonic crystals containing a defect layer with a negative refractive index" *Physical Review E,* vol. 71, no. 6, 13 June 2005, https://doi.org/10.1103/PhysRevE.71.066604.
23. Fink Y., *et al.* "A Dielectric Omnidirectional Reflector" *Science,* vol. 282, no. 5394, 27 November 1998, pp. 1679–1682. https://doi.org/10.1126/science.282.5394.1679.
24. Ellmer K., *et al.,* editors. "Transparent Conductive Zinc Oxide." Springer, 2008.
25. Chen, L., *et al.* "Influence of Absorption Layer Thickness on the Performance of CIGS Solar Cells." *IOP Conference Series: Earth and Environmental Science,* vol. 440, 2020, https://doi.org/10.1088/1755-1315/440/3/032051.
26. Chacko, V., *et al.* "Effect of dispersion on omnidirectional reflection band in zinc oxide-based one dimensional photonic crystal heterostructures." *Journal of Nanophotonics,* vol. 12, no. 2, 8 June 2018, https://doi.org/10.1117/1.JNP.12.026012.
27. "Effect of Temperature." *PVEducation,* www.pveducation.org/pvcdrom/solar-cell-operation/effect-of-temperature. Accessed 9 March 2024.
28. Malik, J. V., *et al.* "Effect of Temperature on Photonic Band Gaps in Semiconductor-Based One-Dimensional Photonic Crystal." *Advances in Optical Technologies,* vol. 2013, no. 2013, 29 August 2013, pp. 1-8. https://doi.org/10.1155/2013/798087.
29. Srivastava, S.K. and Ojha, S.P.. "Reflection and anomalous behaviour of refractive index in defect photonic band gap structure." *Microwave and Optical Technology Letters,* vol. 38, no. 4, 27 June 2003, pp. 293-297. https://doi.org/10.1002/mop.11041.
30. Srivastava, S., *et al.* "Enhancement of Omnidirectional Reflection Bands in One-Dimensional Photonic Crystals with Left-Handed Materials" *Progress In Electromagnetics Research,* vol. 68, 15 September 2007, pp. 91-111. https://doi.org/10.2528/PIER06061602.
31. Chacko, V. "ODR-1DPC." *GitHub,* 16 July 2023, github.com/vinodchacko122345/ODR-1DPC.git. Accessed 9 March 2024.
32. Ojha, S. P., *et al.* "Group velocity, negative and ultra high index of refraction in photonic band gap materials." *Microwave and Optical Technology Letters,* vol. 42, no. 1, 3 May 2004, pp. 82-87. https://doi.org/10.1002/mop.20216.
33. Chacko, V. "Modelling and optimisation of one-dimensional photonic crystal for optical waveguides and devices." *JC Bose University of Science and Technology,* September 2020. dspace-jcboseust.refread.com/xmlui/handle/123456789/657. Accessed 9 March 2024.
34. Aspnes, D.E. and Studna, A. A. "Dielectric functions and optical parameters of Si, Ge, GaP, GaAs, GaSb, InP, InAs and InSb from 1.5 to 6.0 eV." *Physical Review B,* vol. 27, no. 2, 15 January 1983, https://doi.org/10.1103/PhysRevB.27.985.
35. Yeh, P. *Optical Waves in Layered Media.* Wiley Series in Pure and Applied optics, John Wiley and Sons, 25 February 2005, Accessed 11 March 2024

Appendix 1

```
clear;

ios=sqrt(-1);
angles=0;   %angle of incidence from the ambient layer
o1s=1;
thetas=pi.*angles./180;
mts=-1;  %-1for TE and 1 for TM
nls=8;   % NO. OF CELLS
n1s=1;  %refractive index of the ambient medium
d1s=800/(4*3.42);
d2s=800/(4*1.45);
rrs=[3.42,1.45,3.42,1.45,3.42,1.45,3.42,1.45];
ris=[0,0,0,0,0,0,0,0];
ds=[d1s,d2s,d1s,d2s,d1s,d2s,d1s,d2s];
dls=0;
for wls=400:.1:2000
 for is=1:nls
 rinds(is)=complex(rrs(is),-ris(is));
 dls=dls+ds(is);
end
theta1s=(asin(n1s*sin(thetas)/rinds(1)));
theta2s=(asin(rinds(1)*sin(theta1s)/rinds(2)));
thetaas=[theta1s,theta2s,theta1s,theta2s,theta1s,theta2s,theta1s,theta2s];
rks=2*pi/wls;
for ejs=1:nls
 aks(ejs)=(rks*rinds(ejs)*cos(thetaas(ejs)));
end
if(mts<00)
 etaas=(aks(nls-1)/aks(nls));
else
 etaas=((aks(nls-1)/aks(nls))*((rinds(nls)^2/rinds(nls-1)^2)));
end
for oos=2:nls
 iis=oos-1;
ps=(exp(ios*aks(iis)*ds(iis))*(cos(aks(oos)*ds(oos))+(0.5*ios*(etaas+(1/etaas))*sin(aks(oos)*ds(oos)))));
qs=(exp(-ios*aks(iis)*ds(iis))*(0.5*ios*(etaas-(1/etaas))*sin(aks(oos)*ds(oos))));
rs=(exp(ios*aks(iis)*ds(iis))*(-0.5*ios*(etaas-(1/etaas))*sin(aks(oos)*ds(oos))));
ss=(exp(-ios*aks(iis)*ds(iis))*(cos(aks(oos)*ds(oos))-(0.5*ios*(etaas+(1/etaas))*sin(aks(oos)*ds(oos)))));
kws=(1/dls)*acos((cos(aks(iis)*ds(iis))*cos(aks(oos)*ds(oos)))-
(0.5*(etaas+(1/etaas))*(sin(aks(iis)*ds(iis))*sin(aks(oos)*ds(oos)))));
end
kw1ste6(o1s)=kws*dls/(2*pi);
vinste6=[ps,qs;rs,ss]^nls;
ref1ste6(o1s)=(abs((vinste6(3)/vinste6(1))))^2;
trns1ste6(o1s)=1-ref1ste6(o1s);
w1ste6(o1s)=wls;
o1s=o1s+1;
end


ios=sqrt(-1);
angles=90;%angle of incidence from the ambient layer
o1s=1;
```

```
thetas=pi.*angles./180;
mts=1;    %-1for TE and 1 for TM
nls=8;    % NO. OF CELLS
n1s=1;    %refractive index of the ambient medium
d1s=800/(4*3.42);
d2s=800/(4*1.45);
rrs=[3.42,1.45,3.42,1.45,3.42,1.45,3.42,1.45];
ris=[0,0,0,0,0,0,0,0];
ds=[d1s,d2s,d1s,d2s,d1s,d2s,d1s,d2s];
dls=0;
for wls=400:.1:2000
 for is=1:nls
 rinds(is)=complex(rrs(is),-ris(is));
 dls=dls+ds(is);
end
theta1s=(asin(n1s*sin(thetas)/rinds(1)));
theta2s=(asin(rinds(1)*sin(theta1s)/rinds(2)));
thetaas=[theta1s,theta2s,theta1s,theta2s,theta1s,theta2s,theta1s,theta2s];
rks=2*pi/wls;
for ejs=1:nls
 aks(ejs)=(rks*rinds(ejs)*cos(thetaas(ejs)));
end
if(mts<00)
 etaas=(aks(nls-1)/aks(nls));
else
 etaas=((aks(nls-1)/aks(nls))*((rinds(nls)^2/rinds(nls-1)^2)));
end
for oos=2:nls
 iis=oos-1;
ps=(exp(ios*aks(iis)*ds(iis))*(cos(aks(oos)*ds(oos))+(0.5*ios*(etaas+(1/etaas))*sin(aks(oos)*ds(oos)))));
qs=(exp(-ios*aks(iis)*ds(iis))*(0.5*ios*(etaas-(1/etaas))*sin(aks(oos)*ds(oos))));
rs=(exp(ios*aks(iis)*ds(iis))*(-0.5*ios*(etaas-(1/etaas))*sin(aks(oos)*ds(oos))));
ss=(exp(-ios*aks(iis)*ds(iis))*(cos(aks(oos)*ds(oos))-(0.5*ios*(etaas+(1/etaas))*sin(aks(oos)*ds(oos)))));
kws=(1/dls)*acos((cos(aks(iis)*ds(iis))*cos(aks(oos)*ds(oos)))-
(0.5*(etaas+(1/etaas))*(sin(aks(iis)*ds(iis))*sin(aks(oos)*ds(oos)))));
end
kw1stm4(o1s)=kws*dls/(2*pi);
vinstm4=[ps,qs;rs,ss]^nls;
ref1stm4(o1s)=(abs((vinstm4(3)/vinstm4(1))))^2;
trns1stm4(o1s)=1-ref1stm4(o1s);
w1stm4(o1s)=wls;
o1s=o1s+1;
end

plot(w1stm4,ref1stm4,'b',w1ste6,ref1ste6,'r')
title('ODR in  (Si-SiO2) N=8 at lo=800nm')
xlabel('Wavelength (nm)')
ylabel('Reflectivity')
legend('TE','TM')
```

Appendix 2

```
clear;

l1=945;
l2=1206;
```

```
i=1;
for k= l1:.00001:l2
wl(i)=k;
i=i+1;
end
n=i-1;
hc=1.98644568*10^(-25);
sum=0;
j=1;
for j=wl(1):.00001:wl(n)
   sum=sum+(hc/j);
end
sum1=sum/(10^(-9))
```